Rubber Cord Adhesion Inflation Test: Effect of constitutive rubber model on evaluation of Gc

K. Kane, J. Jumel, A. Mbiakop-Ngassa, F. Lallet, Jean-Michel Vacherand, Martin E. R. Shanahan

▶ **To cite this version:**

K. Kane, J. Jumel, A. Mbiakop-Ngassa, F. Lallet, Jean-Michel Vacherand, et al.. Rubber Cord Adhesion Inflation Test: Effect of constitutive rubber model on evaluation of Gc. Engineering Fracture Mechanics, 2021, pp.107547. 10.1016/j.engfracmech.2021.107547 . hal-03480173

HAL Id: hal-03480173
https://hal.science/hal-03480173

Submitted on 13 Feb 2023

HAL is a multi-disciplinary open access archive for the deposit and dissemination of scientific research documents, whether they are published or not. The documents may come from teaching and research institutions in France or abroad, or from public or private research centers.

L'archive ouverte pluridisciplinaire **HAL**, est destinée au dépôt et à la diffusion de documents scientifiques de niveau recherche, publiés ou non, émanant des établissements d'enseignement et de recherche français ou étrangers, des laboratoires publics ou privés.

Distributed under a Creative Commons Attribution - NonCommercial 4.0 International License

Version of Record: https://www.sciencedirect.com/science/article/pii/S0013794421000242
Manuscript_836a2a9aae08844b405e19d5c5d292cd

Rubber Cord Adhesion Inflation Test: Effect of constitutive rubber model on evaluation of G_c

K. Kane[*,1,2], J. Jumel[†1,3,4], A. Mbiakop-Ngassa[2], F. Lallet[2], Jean-Michel Vacherand[2], Martin E.R. Shanahan[1,3,4]

[1]I2M, University of Bordeaux, UMR 5295, 33400 Talence, France.

[2]Manufacture française des pneumatiques MICHELIN, Site de Ladoux, 23 place Carmes Déchaux, 63040 Clermont-Ferrand, France.

[3]CNRS, I2M, UMR 5295, F-33400 Talence, France.

[4]Arts et Métiers Paris Tech, I2M, UMR 5295, F-33400 Talence, France

Abstract:

The Rubber Cord Adhesion Inflation Test (RCAIT) is a recently proposed test protocol to study tyre rubber-steel cord fracture [1]. As in the traditional blister test, a pressurised fluid is injected between the two adherends to propagate fracture. The fracture energy, G_c, is directly related to the strain energy stored in the inflated rubber. It was shown that evaluation of G_c for RCAIT depends intimately on how well the hyperelastic model is capable of predicting the rubber inflation condition [2]. Here, a thick tube inflation model is proposed for a generalised, phenomenological, hyperelastic material. It is subsequently applied to RCAIT in order to study which data processing technique is likely to be the most reliable to evaluate the critical strain energy release rate of the specimen.

[*] Corresponding author: Kaustubha Kane, kaustubha.kane@u-bordeaux.fr

[†] Presently at : ENSTA Bretagne, 2 rue François Verny, 29200, Brest, France

© 2021 published by Elsevier. This manuscript is made available under the CC BY NC user license
https://creativecommons.org/licenses/by-nc/4.0/

Nomenclature

c : Integration constant

G, G_c : Strain Energy Release Rate, Critical Strain Energy Release Rate

F_z : Axial force

I_1, I_2, I_3 : First, second and third invariant of strain

l_p : Pre-crack length of the specimen

P : Fluid inflation pressure

p : Hydrostatic pressure component

P_{int}, P_{ext} : Pressure at the internal and external surface of the specimen

R_{tube} : Inner radius of the confinement tube

r, r_0 : Radial position- deformed, undeformed

r_0^{int}, r_0^{ext} : Inner, outer initial rubber envelope radii (undeformed state)

r^{int}, r^{ext} : Inner, outer rubber envelope radii (deformed state)

u : Radial position variable for integration

W : Strain energy density function

z, z_0 : Axial position- deformed, undeformed

δ : Hydrostatic distribution

λ_1, λ_2, λ_3 : Principal stretch ratios along the three coordinate axes

λ_r, λ_θ, λ_z : Radial, circumferential and axial stretch ratio

σ_i^{dev} : Deviatoric part of the Cauchy stress

σ_{rr}, $\sigma_{\theta\theta}$, σ_{zz} : Radial, circumferential and axial component of the Cauchy stress tensor

χ_{fluid} : Fluid compressibility

CIS : Confined Inflation Stage

RCAIT : Rubber Cord Adhesion Inflation Test

SERR : Strain Energy Release Rate

UIS : Unconfined Inflation Stage

1. Introduction

Tyres are complex structures that function as the key components to give road vehicles the control and stability required for a smooth ride both on and off road. The entire weight of the vehicle, along with the torsional and frictional forces arising from power application, braking and steering are supported by the tyres. Apart from these mechanical loads, a tyre has to withstand deleterious effects due to heat and humidity during its entire life, whether the vehicle is operational or not. Therefore, for the safety of the vehicle and its surroundings, tyre designers have to insist on the safety of tyres.

Designing safe tyres starts from understanding how different components of the tyres withstand all these loads. A tyre is made up of different layers such as fabric, polymers and metal cable mesh, that are embedded in a rubber matrix. Each of these layers serves a distinct purpose. One very important layer is that of the metal cable mesh. This metal cable layer gives the tyre its rigidity and structure [3]. Safety of the tyre is largely dependent on how well this composite material made up of rubber matrix and metal reinforcement performs under various loads and environmental factors.

During the vulcanization process of the tyre, the rubber matrix and metal reinforcement adhere as a result of strong Cu-S covalent bonds [4], [5]. These bonds create a dendritic structure that produces physico-chemical adhesion between the two materials *via* a brass coating deposited on the metal cable prior to the vulcanization. For a tyre designer, developing strong rubber-metal adhesion is therefore essential to produce a strong, durable tyre. The only way to evaluate the strength of this adhesion is to perform fracture mechanics tests on the rubber-metal composite.

Rubber-metal adhesion is a complex topic to study since it involves both nonlinear materials and adhesion, as well as effect of environmental parameters on the adhesive interface [6].

Several fracture mechanics tests have been proposed and used in the tyre industry as standard procedures, such as those presented in [7] - [18]. These tests can be mainly divided into two groups *viz.* wire pull-out tests and peel tests. Peel tests fail to mimic the cylindrical nature of the rubber-metal adhesion layer. This is because the brass coating deposited on the metal cord during the wire drawing process cannot be accurately represented by brass coating on a planar, peel test specimen. Moreover, the pull-out geometry suffers from rubber-metal friction losses during the tests, which affects the evaluation of the fracture energy. Therefore, to overcome these experimental artefacts, a rubber-metal cord fracture test *viz.* Rubber Cord Adhesion Inflation Test (RCAIT) was recently proposed [1].

The RCAIT protocol is an axisymmetric version of the blister test used for film-substrate delamination [19]. The test specimen is in the shape of a rubber cylinder with the metal cord embedded along the central axis. The test protocol consists of injecting a pressurised fluid between the rubber and the metal cord to provoke fracture. A coaxial confinement tube restricts the inflation of the rubber allowing the fracture to propagate along the rubber-metal interface. A similar approach was used in the case of a constrained blister test in [20] and [21].

For a quantitative analysis of the rubber-metal adhesion by RCAIT, a global energy balance was proposed in [1]. It was shown that the energy stored in the pressure-inflated rubber constitutes a major part of the fracture energy evaluation. In [1] and [2] the energy stored in the pressure-inflated rubber was calculated for a Mooney-Rivlin rubber and an Ogden rubber respectively. It was found that inaccurate evaluation of rubber tube deformation can lead to substantial errors in the specimen critical SERR evaluation. With these results in mind, this article investigates the influence of rubber behaviour modelling and identification method on the evaluation of thick tube inflation. The final objective is to obtain a reliable estimate of the SERR during RCAIT so that only measurable quantities need to be considered. A similar

study of various rubber models and how well they can represent tensile test or shear test data has been carried out in [22] and [23]. In addition, in [24], [25] and [26], a review of various hyperelastic models, their stress-strain relations and some experimental results are presented.

In the first section of this work, a brief introduction of RCAIT and representative results of one test are given. The global energy balance to calculate fracture energy (critical SERR) is briefly described. The critical SERR value calculated using the experimental data is also presented. Further, a semi-analytical resolution technique is proposed to simulate thick tube inflation in the case of incompressible hyperelastic materials, as an alternative to other approaches such as those presented in [27] and [28]. Various strategies are then used to identify the rubber and tube inflation behaviour from a simple set of experimental data. A generalised critical (SERR) equation is presented, based on this theoretical model. Finally, following the framework of [22] and [23], the critical SERR of the rubber-metal interface is evaluated using several hyperelastic models. Various identification protocols to evaluate the sensitivity of G_c estimation with respect to the data processing are also presented.

2. Rubber Cord Adhesion Inflation Test (RCAIT)

In RCAIT, the test specimen is a cylindrical envelope made from rubber having an axial steel cord adhered to the rubber. A small pre-crack is created while preparing the specimen so that a pressurised fluid can be injected between the rubber and the metal. A coaxial glass tube is

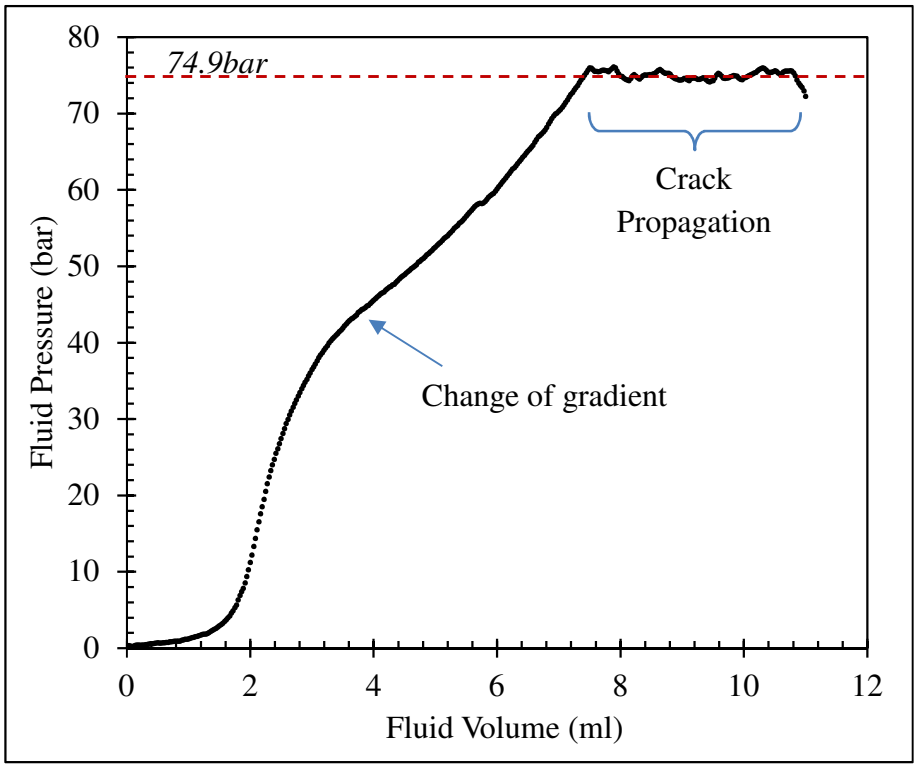

Figure 2: Typical Pressure vs Volume plot of RCAIT specimen

used to confine the rubber envelope and to restrict the radial inflation. The confinement tube ensures that the rubber does not inflate unstably, and the pressurised fluid causes the rubber to inflate axially. A schematic diagram of the test protocol is shown in *Figure 1*. As more fluid is injected, the pressure increases, and the rubber envelope inflates in both axial and radial directions. Eventually the fluid pressure reaches a plateau value and the crack propagates

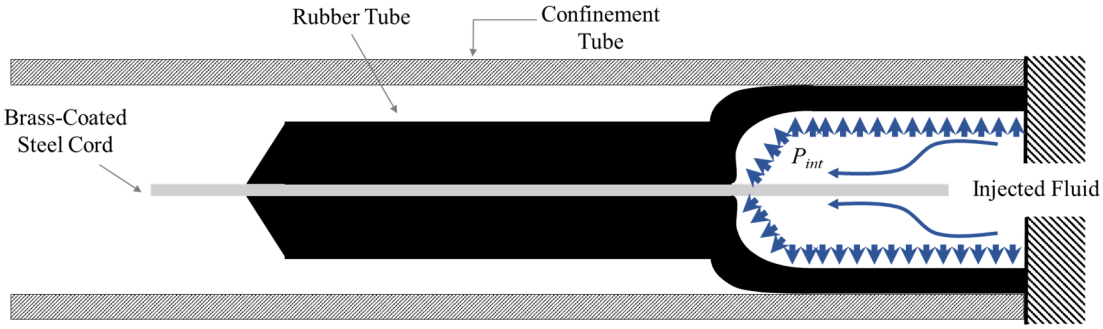

Figure 1: Schematic of the Rubber Cord Adhesion Inflation Test

along the interface.

A typical fluid pressure response recorded in a RCAIT is shown in *Figure 2*. The specimen consists of a rubber envelope of length *100mm*, inner radius *0.65mm* and outer radius *4.7mm* and adhered to a brass coated steel cord of diameter *1.3mm* along the axis. The average thickness of the brass coating is in the range of *0.05 to 0.1μm*. An anti-adhering tape is used to cover *50mm* length of the steel cord to produce initial debonding, or a pre-crack. The rubber envelope is made from natural rubber with *65phr* of carbon black and *4.5phr* of sulphur. The fluid (water) is injected inside the specimen at a rate of *5ml/min* using a syringe pump. A hydraulic system connects the specimen to the syringe. Injected volume is determined from the piston displacement value, while a sensor is used to measure the pressure of the injected fluid. Initially, the rubber envelope inflates radially and axially until it touches the confinement tube (up to approx. *50bar*). Once the rubber envelope comes in contact with the confinement tube, the rigid confinement tube restricts the external radius of the rubber tube from expanding further. Being incompressible, the rubber is then forced to stretch axially, and radially only at the inner radius. This changes the 'gradient' of the *Pressure vs Volume* curve, as seen in *Figure 2*. Eventually, the fluid pressure reaches a plateau value and the crack propagates along the interface.

2.1. Global Energy Balance

The aim of RCAIT is to evaluate the fracture energy required to propagate a crack along the rubber metal interface from the test data (pressure evolution). This can be done by a simple global energy balance. Some of the details already presented in detail in [1] are recalled here.

The test is divided into three regimes: (a) Unconfined Inflation Stage (UIS) (b) Confined Inflation Stage (CIS) (c) Interface Fracture Stage (IFS). The total energy put into the test specimen is that supplied by the fluid injected. Part of this input is stored in the inflated

rubber; part is stored in the fluid itself as the potential energy of compression and the rest is liberated as fracture energy. This can be written in an equation form as

$$W_{PdV} = E_{rubber} + E_{compressibility} + E_{fracture}$$

$$G_c * A_{fracture} = E_{fracture} = W_{PdV} - E_{rubber} - E_{compressibility}$$

where G_c is critical SERR and $A_{fracture}$ is the area of the fractured surface. W_{Pdv} is the work input to the test specimen, $E_{compressibility}$ is the amount of energy stored in the compressed fluid at the pressure P and E_{rubber} is the energy stored in the inflated rubber during the UIS and CIS. The terms W_{Pdv} and $E_{compressibility}$ can be calculated directly using their definitions. Therefore, if the term E_{rubber} is calculated precisely, the fracture energy or G_c ($E_{fracture}/A_{fracture}$) can be calculated without any experimental artefacts. This task is, in fact, complex since the rubber undergoes complex loading conditions as well as finite deformation. Therefore, preliminary analysis should be performed to identify which models are most sensitive to capture the rubber tube inflation response during the RCAIT in relation to the behaviour observed in the traditional tensile tests.

It should be noted that it is possible to calculate G_c without any consideration of rubber material behaviour. It was shown in [1] that the share of $E_{compressibility}$ is negligible in the energy balance for nearly incompressible fluids such as water. The quantity E_{rubber} can be calculated using the area under the curve in the inflation regime of *Figure 2*. This energy is stored in the entire pre-crack length of the specimen (*50mm*). Similarly, W_{PdV} can be calculated as described in [2]. It is stored in the fractured length of the specimen, *i.e. 50mm*. For the test shown in *Figure 2*, E_{rubber} is *27.3J* and W_{PdV} is *32.9J*. Therefore, following the energy balance presented above, the critical SERR is $27.4 kJm^{-2}$.

Although this method of calculating critical SERR is simple, it is susceptible to errors. The rate of deformation of the pre-crack length of the specimen is different from that of the

fractured length of the specimen. The pre-crack length of the specimen undergoes a steady increase in inflation pressure and volume, from zero at the start of the test, to a certain pressure (*74.9bar*) and volume (*7.38ml*) until crack initiation. On the other hand, the fractured length of the specimen undergoes sudden inflation at a nearly constant crack propagation pressure (*74.9bar*). Therefore, the E_{rubber} values in these two regions of the specimen are likely to be different. However, in the calculation presented above, they are assumed to be equal. Any errors in the experimental data caused by inaccuracies in pre-crack length or the presence of trapped air in the hydraulic circuit will greatly affect G_c calculation. Moreover, this method of G_c calculation does not consider directly any microscopic parameters of the crack propagation such as viscoelastic dissipation in the bulk rubber or near the crack tip in the form of a process zone. Therefore, by formulating a theoretical or semi-analytical model, precise evaluation of E_{rubber} can be achieved. Such a model, in the future, may be improved by considering the viscoelastic dissipation in the bulk rubber as well.

In this context, the present work focuses on evaluating E_{rubber} using a semi-analytical model and investigating its effect on the calculation of G_c. The Thick Rubber Tube Inflation Model proposed previously in [2] to calculate E_{rubber} for an Ogden type rubber can be extended to various phenomenological hyperelastic models applied to the fracture problem. In the following section, an alternative semi-analytical resolution technique is proposed which is applicable to a large variety of rubber models.

3. Thick-Walled Cylinder Inflation Model

The strain energy stored in the rubber tube itself (E_{rubber}) needs to be evaluated in order to solve the problem of a thick incompressible hyperelastic closed-ended tube, confined and

loaded under internal pressure. The procedure proposed below is applicable for any type of incompressible hyperelastic material.

3.1. Constitutive equations

Consider an infinitely long thick rubber cylinder with inner radius and outer radius respectively r_0^{int} and r_0^{ext}. Due to the inflation pressure, the cylinder expands both axially and radially so that in the deformed state the inner and outer radii are respectively r^{int} and r^{ext}. During the inflation loading the deformation and displacements are assumed to be large. Due to the geometry of the rubber envelope, the problem to be solved is axisymmetric. Therefore, polar coordinates are used, and the displacement field is expressed using only two functions: $u_r(r)$ and $u_z(r)$. No θ dependence is assumed as the deformation is homogeneous. In the following analysis, a Lagrangian description is preferred so that rather than evaluating displacements, the calculation aims at updating the position. (r_0, z_0) refers to the initial position while (r, z) refers to the position in the deformed state. Uniform deformation along the tube is assumed so that no z dependence is considered here, and the deformation field is expressed as a function of radius only. With these assumptions the material elongation (stretches) in the tube are given by relations:

$$\lambda_r(r) = \frac{dr}{dr_0} \qquad \lambda_\theta(r) = \frac{r}{r_0} \qquad \lambda_z = \frac{z}{z_0} \tag{1}$$

For incompressible hyperelastic materials condition $\lambda_r\lambda_\theta\lambda_z = 1$ is applicable. Assuming a uniform λ_z value due to homogenous deformation, explicit expressions for the radial evolution of principal stretches can be obtained:

$$\lambda_r{}^2(r) = \frac{1}{\lambda_z}\left[\frac{cr^2 - 1}{cr^2}\right] \tag{2}$$

$$\lambda_\theta{}^2(r) = \frac{1}{\lambda_z}\left[\frac{cr^2}{cr^2 - 1}\right] \tag{3}$$

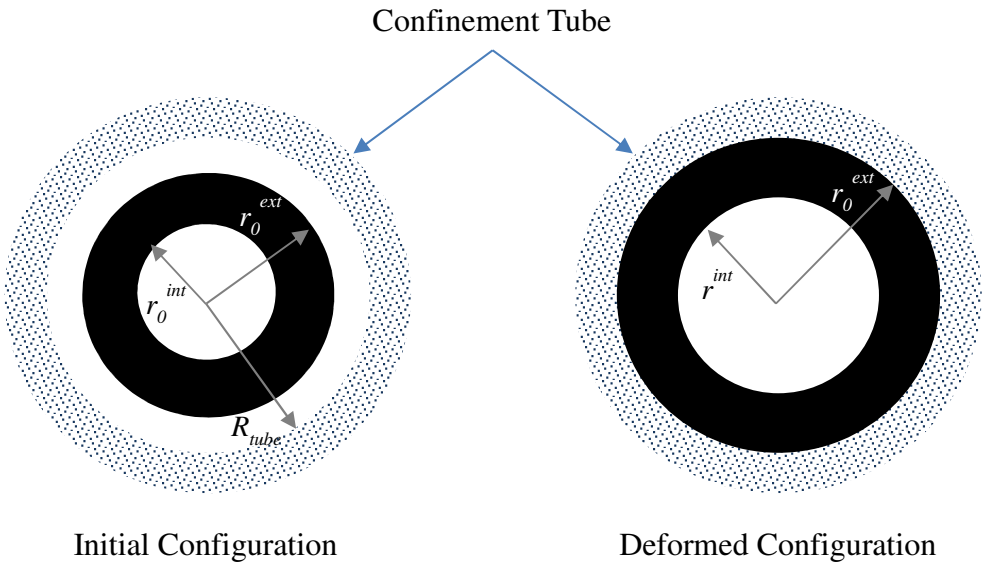

Figure 3: Cross section of the rubber tube and the coaxial confinement tube

$$r = \sqrt{\frac{1}{c} + \frac{{r_0}^2}{\lambda_z}} \tag{4}$$

c is an integration constant related to the deformation. Details of the intermediate calculations are given in [29].

Consider the stress equilibrium equation in axisymmetric mode, as shown in *Figure 3*. Due to the axisymmetric geometry no shear components are considered, and the stress tensor reduces to only three components σ_r, σ_θ and σ_z in radial, circumferential and axial direction respectively. The equilibrium equations in polar coordinates reduce to the relation:

$$\frac{d\sigma_{rr}}{dr} + \frac{\sigma_{rr} - \sigma_{\theta\theta}}{r} = 0 \tag{5}$$

The boundary conditions applied to the inflated rubber are as following. A uniform pressure is applied inside the tube by the injected fluid. This results in a uniform normal stress applied to the inner radius but also produces an axial force due to the pressure applied to inner cross section. This leads to the following equations:

$$\sigma_{rr}\left(r^{int}\right) = -P \tag{6}$$

$$2\pi \int_{r^{int}}^{r^{ext}} \sigma_{zz}(u)\, u du = P\pi {r^{int}}^2 \quad (7)$$

Alternatively, it was found that in the case of dry contact, friction forces compensate the axial force exerted by the pressurized fluid. As for the shear lag model, the friction force decreases rapidly from the crack tip so that the stationary regime to consider far from the crack tip is equivalent to an open-end pressurized tube. This leads to the condition:

$$2\pi \int_{r^{int}}^{r^{ext}} \sigma_{zz}(u)\, u du = 0 \quad (8)$$

In the first inflation regime- the UIS- the rubber inflates radially and axially without any confinement. Then in the next stage (CIS), the external radius touches the confinement tube which is lubricated to limit friction. This creates a frictionless rigid contact between the inflated rubber cylinder and the confinement tube. These two stages lead to the following boundary conditions:

$$\sigma_{rr}(r^{ext}) = 0 \text{ for } r^{ext} \leq R_{tube} \quad (9)$$

$$r^{ext} = R_{tube} \quad (10)$$

In practice, imposing an internal pressure value and zero external pressure as boundary conditions renders the resolution of the problem numerically more complex. Therefore, these boundary conditions are replaced by using the internal and external radius in the deformed state as the driving parameters.

3.2. Incompressible Hyperelasticity and the Inflation Model

For the approach presented above to be applicable, the material must be considered to be incompressible. In the following, only hyperelastic models based on phenomenological thermodynamics are considered. Physically based models could also be implemented, though

the stress/stretch relation and potential energy density might be more difficult to derive. This review is not exhaustive since a large number of complex hyperelastic models can be found in the literature but only a few of them are being applied since the test data available for the rubber is limited.

Considering a general, isotropic, incompressible material, the strain energy density function depends only on two invariants I_1 and I_2. I_3 remains constant since it corresponds to the relative volume variation:

$$I_1 = {\lambda_1}^2 + {\lambda_2}^2 + {\lambda_3}^2 \tag{11}$$

$$I_2 = {\lambda_1}^2{\lambda_2}^2 + {\lambda_2}^2{\lambda_3}^2 + {\lambda_1}^2{\lambda_3}^2 \tag{12}$$

$$I_3 = {\lambda_1}^2{\lambda_1}^2{\lambda_3}^2 = 1 \tag{13}$$

For incompressible materials, the true principal (Cauchy) stresses are related to the elongation and invariants by the relations:

$$\sigma_i = 2\left({\lambda_i}^2\frac{\partial W}{\partial I_1} - \frac{1}{{\lambda_i}^2}\frac{\partial W}{\partial I_2}\right) - p \tag{14}$$

$$\sigma_i = -p + \lambda_i\frac{\partial W}{\partial \lambda_i} = -p + {\sigma_i}^{dev} \tag{15}$$

where ${\sigma_i}^{dev}$ is the deviatoric part of the stress.

The following procedure is used to determine all quantities describing the cylindrical rubber envelope expansion under confined or unconfined conditions. First, internal and external radius values are set so that c and λ_z are determined with the relations:

$$\lambda_z = \frac{{r_0}^{ext^2} - {r_0}^{int^2}}{r^{ext^2} - r^{int^2}} \tag{16}$$

$$\frac{1}{c} = \frac{r^{int^2}{r_0}^{ext^2} - r^{ext^2}{r_0}^{int^2}}{{r_0}^{ext^2} - {r_0}^{int^2}} \tag{17}$$

Then using *(1)* the radial and circumferential stretch ratios are determined so that the deviatoric part of the Cauchy stress becomes:

$$\sigma_i{}^{dev} = \lambda_i \frac{\partial W}{\partial \lambda_i} \tag{18}$$

Explicit expressions for the deviatoric stress can easily be derived for most of the phenomenological hyperelastic models. Then, the equilibrium equation *(5)* is used to introduce the hydrostatic pressure evolution:

$$\frac{dp}{dr} = \frac{d\sigma_{rr}{}^{dev}}{dr} + \frac{\sigma_{rr}{}^{dev} - \sigma_{\theta\theta}{}^{dev}}{r} \tag{19}$$

For a given inner and outer radius, the deviatoric part of the stress is known throughout the thickness, and the hydrostatic pressure must be determined using the following integral formulation:

$$p(r) = \sigma_{rr}{}^{dev}(r) - \sigma_{rr}{}^{dev}\left(r^{int}\right) + \int_{r^{int}}^{r} \frac{\sigma_{rr}{}^{dev}(u) - \sigma_{\theta\theta}{}^{dev}(u)}{u} du + p\left(r^{int}\right)$$

$$= \delta(r) + p\left(r^{int}\right) \tag{20}$$

The hydrostatic distribution $\delta(r)$ can be determined numerically using trapezoidal integration. The hydrostatic constant $p(r^{int})$ can then be determined by combining *(7)* and *(20)* as following:

$$F_z = -p\left(r^{int}\right)\pi\left(r^{ext^2} - r^{int^2}\right) + 2\pi \int_{r^{int}}^{r^{ext}} [\sigma_{zz}{}^{dev}(u) - \delta(u)]udu = \pi r^{int^2} P_{int} \tag{21}$$

The fluid pressure P_{int} is given by

$$P_{int} = -\sigma_{rr}\left(r^{int}\right) = p\left(r^{int}\right) - \sigma_{rr}{}^{dev}\left(r^{int}\right) \tag{22}$$

So that:

$$p\left(r^{int}\right) = \frac{r^{int^2}}{r^{ext^2}} \sigma_{rr}{}^{dev}\left(r^{int}\right) + \frac{2}{r^{ext^2}} \int_{r^{int}}^{r^{ext}} [\sigma_{zz}{}^{dev}(u) - \delta(u)]udu \tag{23}$$

Using the $\delta(r)$ value calculated by the trapezoidal integration $p(r^{int})$ is determined numerically using the trapezoidal rule again.

For open-end condition regime, we have:

$$F_z = -p(r^{int})\pi(r^{ext^2} - r^{int^2}) + 2\pi \int_{r^{int}}^{r^{ext}} [{\sigma_{zz}}^{dev}(u) - \delta(u)]udu = 0 \qquad (24)$$

So that:

$$p(r^{int}) = \frac{2}{r^{ext^2} - r^{int^2}} \int_{r^{int}}^{r^{ext}} [{\sigma_{zz}}^{dev}(u) - \delta(u)]udu = 0 \qquad (25)$$

Once the total hydrostatic pressure function *p(r)* is evaluated for a given choice of inner and outer radii, the stress distribution in the entire rubber thickness can be easily obtained. Finally, the inner and outer pressure values are determined by the relations:

$$P_{int} = -\sigma_{rr}\left(r^{int}\right) \qquad P_{ext} = -\sigma_{rr}(r^{ext}) \qquad (26)$$

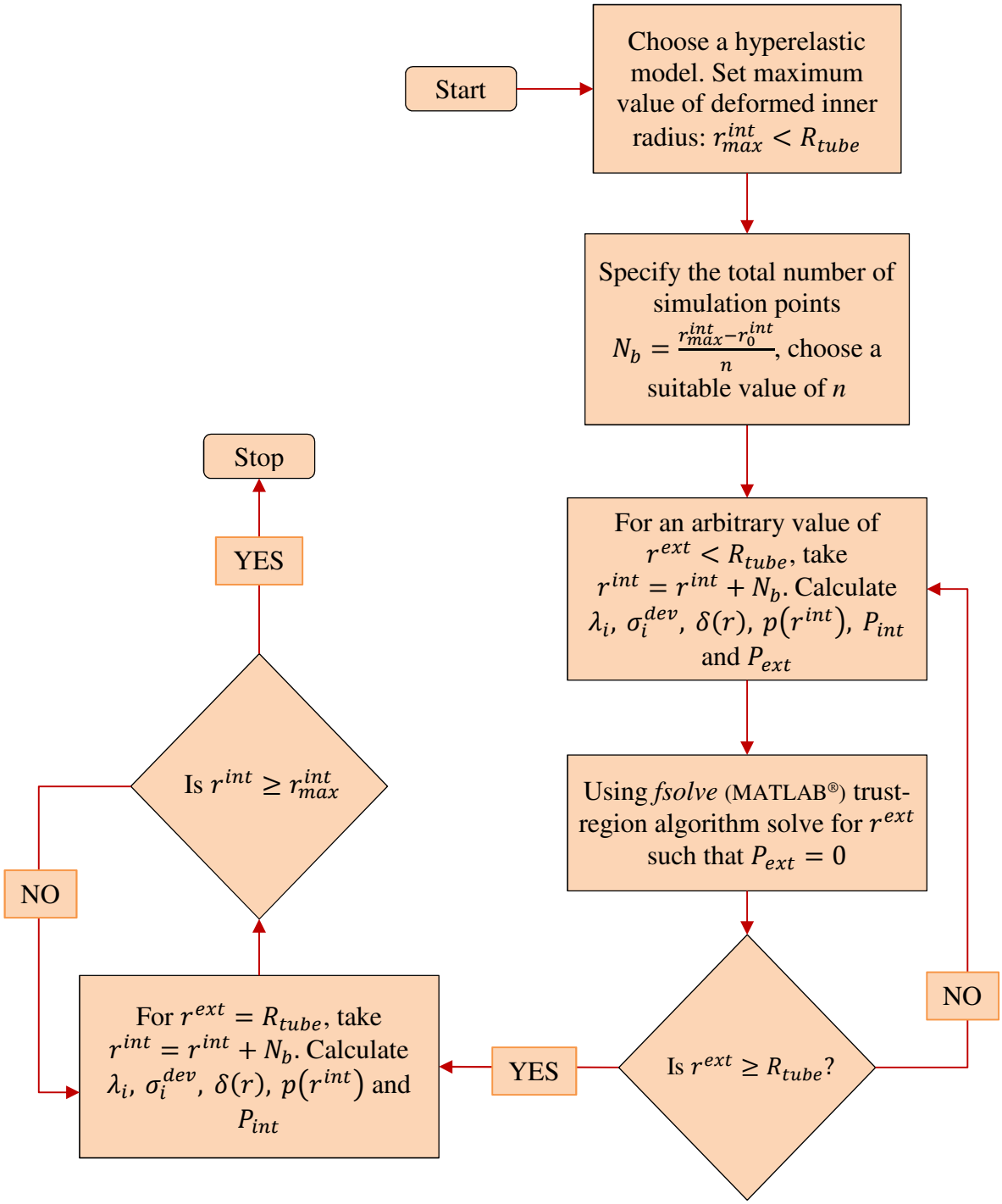

Figure 4: Generalised Thick-Walled Cylinder Inflation Algorithm for hyperelastic materials

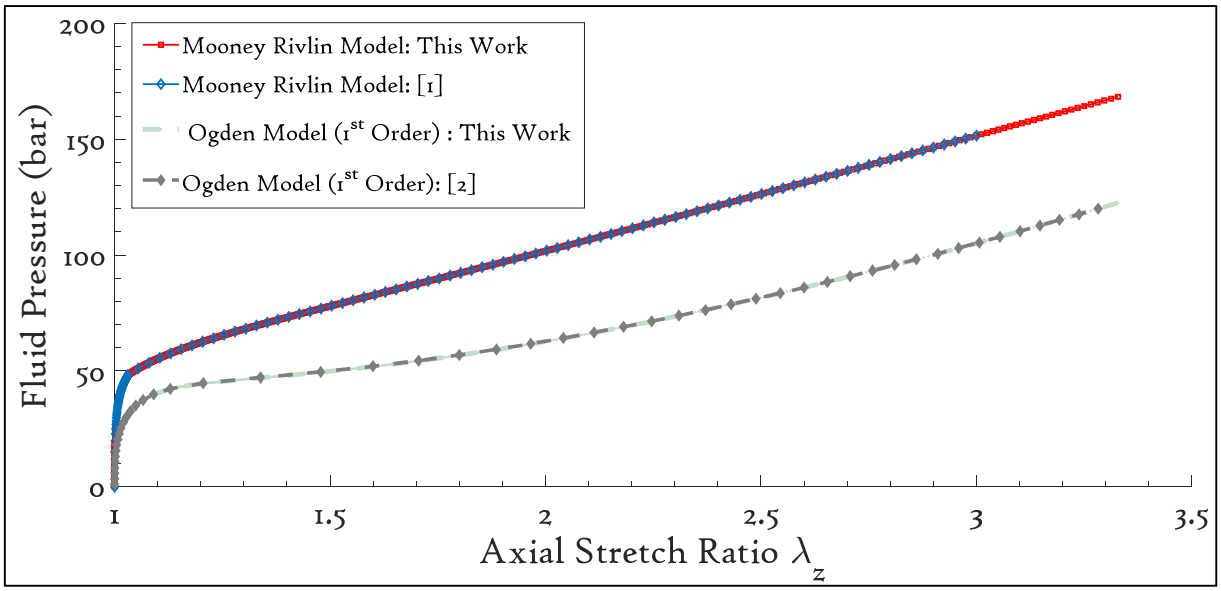

Figure 5: Comparison between Thick-Walled Cylinder Inflation algorithms presented in Figure 4 and in [1] and [2]

In the UIS, an iterative procedure is used to adjust the outer radius r^{ext} so that the stress-free outer surface condition $P_{ext}=0$ is satisfied. In the CIS, the $P(\lambda_z)$ evolution is obtained directly by imposing $r^{ext} = R_{tube}$ and using the above integration procedure.

The algorithm to calculate stress-elongation state of the rubber cylinder at any specified deformed state (r^{int} value) is described in *Figure 4*. r^{int} is the only parameter increasing monotonically during the inflation, therefore it is chosen as the driving parameter.

For applying the algorithm presented in *Figure 4* to a chosen rubber model, stress *vs* stretch ratio relations *(14)* and *(15)* must first be derived. Then, using the algorithm, the through thickness stress - strain distributions are found so that specimen overall deformation can be expressed as a function of applied fluid pressure. In *Figure 5*, theoretical $P(\lambda_z)$ evolution is given for the experimental condition presented in *Figure 2* considering a Mooney-Rivlin Model as well as a 1st order Ogden model. Results obtained by applying the algorithm shown in *Figure 4* are compared with the results presented in [1] and [2]. The rubber material parameters are found by fitting uniaxial tensile test data to the Mooney-Rivlin and Ogden models. The Mooney-Rivlin parameters are $C_1= 1.34MPa$ and $C_2=0.37MPa$; whereas the Ogden parameters are $\alpha=2.64$ and $\mu=1.89MPa$. The two curves plotted using previous and

this work follow the same path for both the material models. In [1] and [2], the semi-analytical model and the algorithm for the Ogden model respectively were cross-checked using a finite element models and were found to be virtually identical. Therefore, *Figure 5* constitutes strong evidence of the results obtained by applying the algorithm shown in *Figure* 4.

Having established the validity of the equations and the algorithm, the specimen fracture energy can now be computed by performing global energy balance analysis as explained above. The equations are given in detail here:

$$\delta W_P = \delta W_{rubber} + \delta W_{fluid} + G_c 2\pi r_0^{int} \delta a \qquad (27)$$

In *(27)*, W_P corresponds to the work provided to the whole system by pressure injection. W_{rubber} is the potential energy stored in the rubber envelope inflation, W_{fluid} is the potential energy stored in fluid compressibility and $G_c 2\pi r_0^{int} \delta a$ is the energy dissipated due to crack propagation of length δa. In *(27)*, proper evaluation of the stored potential energy is of the utmost importance for the reliable evaluation of G_c.

The analysis presented in this work is based on assumptions of linear ELASTIC fracture mechanics in the sense that the crack initiation is assumed to be controlled only by the G_c value, without consideration of any irreversible processes which may occur before the fracture proceeds. Any viscoelastic effects present in the rubber and/or at the interface will be included in the G_c value at this stage. Under such condition, the energy balance described in equation *(27)* is sufficient to evaluate the energy needed to propagate the crack. However, it is important to note that the extent of the process zone ahead of the crack tip is not exactly known. Also, the specimen envelope deformation controls the stress/strain distribution in the near crack tip vicinity and consequently the damage process.

In *(27)* the various terms are given as following:

$$\delta W_P = P_{int}\pi\left(r^{int^2} - r_0^{int^2}\right)\lambda_z\delta a \tag{28}$$

$$\delta W_{rubber} = \int_{r^{int}}^{r^{ext}} \delta w(r) 2\pi r dr\, \lambda_z \delta a \tag{29}$$

$$\delta W_{fluid} = \frac{1}{2}\frac{P_{int}^2}{\chi_{fluid}}\pi\left(r^{int^2} - r_0^{int^2}\right)\lambda_z\delta a \tag{30}$$

Combining *(27)-(30)* gives following relation for energy balance

$$\left(\frac{P_{int}}{2} - \frac{1}{4}\frac{P_{int}^2}{\chi_{fluid}}\right)\left(r^{int^2} - r_0^{int^2}\right)\lambda_z - \int_{r^{int}}^{r^{ext}} \delta w(u) u du\, \lambda_z = G_c r_0^{int} \tag{31}$$

(31) can be rearranged to get

$$G_c = \frac{\lambda_z}{r_0^{int}}\left[\left(\frac{P_{int}}{2} - \frac{P_{int}^2}{4\chi_{fluid}}\right)\left(r^{int^2} - r_0^{int^2}\right) - \int_{r^{int}}^{r^{ext}} \delta w(u) u du\right] \tag{32}$$

(32) holds true for any hyperelastic model (neglecting dissipation mechanisms) applied to the rubber cylinder. By following the procedure described earlier the stress-elongation state of the rubber cylinder can be calculated for any type of hyperelastic material. It can then be used to solve the integral $\int_{r^{int}}^{r^{ext}} \delta w(u) u du$ using Riemann Sum or Trapezoidal Rule or any other numerical integration method.

4. Application to various rubber models

Since the proper evaluation of rubber envelope deformation is fundamental for reliable determination of G_c, proper identification of the rubber behaviour is also fundamental. Therefore, it is interesting to investigate how various rubber models can be used to describe the complex inflation problem and how they affect the value of critical SERR (G_c) evaluated using *(32)*. In [22] and [23] a similar study was done on various hyperelastic models to compare their performance on Uniaxial, Biaxial and pure shear data reported by Treloar in [30].

4.1. Uniaxial test data fitting

Numerous hyperelastic models are available in the literature out of which *10* different models were fitted to the tensile test data of the rubber and it was found that five models show the least residual values signifying a good fit. These models are: Mooney-Rivlin [31], Ogden Model [32], Yeoh Model [33], Lopez-Pamies Model [34] and ExpLn Model [35]. Of these, *Mooney-Rivlin Model* and *Ogden Model* (1st Order) were already used in [1] and [2] respectively, to describe the thick walled cylinder inflation of the rubber under consideration.

For the tensile test data, a dumbbell specimen was cut from a sheet of the same rubber used in the specimen of *Figure 2*. It was loaded under tension at a constant displacement rate of *5mm/min* or a constant strain rate of 0.22×10^{-2}/s. Using the *lsqnonlin* algorithm of *MATLAB*®, the Cauchy stress *vs* stretch ratio data were fitted to the five models. It should be remembered that the *Ogden*, *Yeoh* and *Lopez-Pamies* models are expressed as a series sum. The strain energy density terms can be written as 1st order, 2nd order, 3rd order and so on. In this work, only the first 3 orders of the strain energy density functions are considered for *Ogden* and *Lopez-Pamies* models. The *Yeoh* model is used in its 2nd and 3rd order only. The 1st order *Yeoh* model is equivalent to a *Neo-Hookean* solid which shows a very poor fit due to the absence of

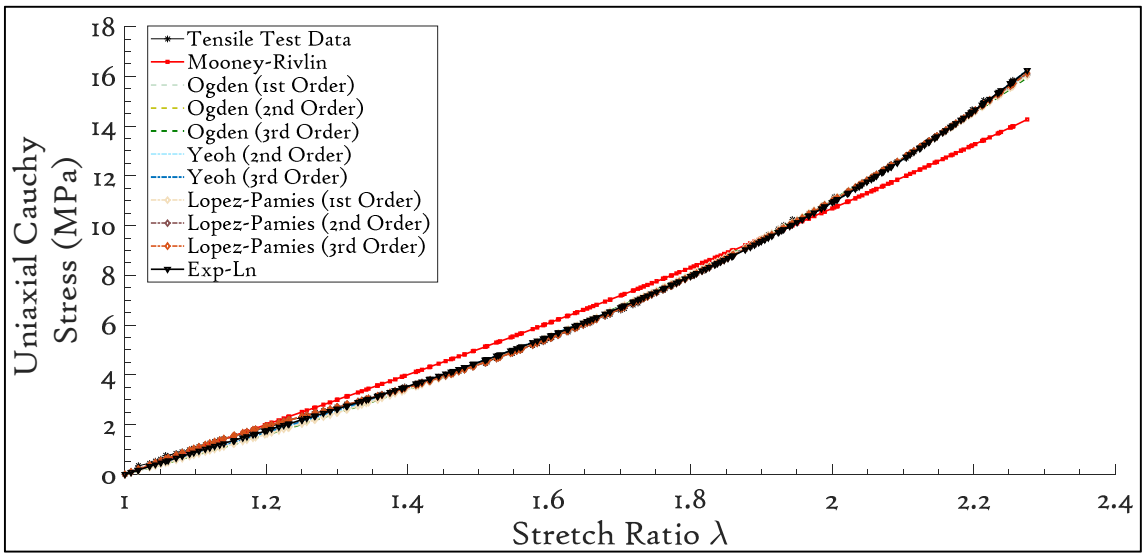

Figure 6: Uniaxial tensile test fit for the five models

a strain hardening factor, as well as I_2 independence. Hence it is omitted in this work. Therefore, in total there are 10 hyperelastic Cauchy stress functions to be fitted to the tensile test data.

The uniaxial tensile data fitted to these 10 stress functions are shown in *Figure 6*. Due to the absence of a strain hardening parameter, the *Mooney-Rivlin* model does not fit well at moderate and large strains. Overall, the other four models seem to fit to the data well at small

Hyperelastic Model	**Parameter fit from Uniaxial Tests**	
Mooney-Rivlin	C_1=1.34 MPa	C_2=0.37MPa
Ogden Model (1st Order)	α=2.64	μ=1.89MPa
Ogden Model (2nd Order)	α_1=0.175	μ_1=4.97MPa
	α_2=2.81	μ_2=1.52MPa
Ogden Model (3rd Order)	α_1=0.0075	μ_1=8.4MPa
	α_2=2.67	μ_2=1.81MPa
	α_2=0.0074	μ_2=23MPa
Yeoh Model (2nd Order)	C_1=1.33MPa	C_2=0.059MPa
Yeoh Model (3rd Order)	C_1=1.39MPa	C_2=0.024MPa
	C_3=0.006MPa	
Lopez-Pamies Model (1st Order)	α=1.36	μ=2.62MPa
Lopez-Pamies Model (2nd Order)	α_1=1.41	μ_1=2.54MPa
	α_2=-16.26	μ_2=1.11MPa
Lopez-Pamies Model (3rd Order)	α_1=1.06	μ_1=1.31MPa
	α_2=1.68	μ_2=1.26MPa
	α_2=-17.7	μ_2=1.12MPa
ExpLn	A=1.16MPa	a=0.102 b=-0.02

Table 1: Uniaxial test data fit to 10 Cauchy stress equations (5 hyperelastic models)

as well as large strains. The strain energy density parameters calculated for each of the 10 cases are tabulated in *Table 1*.

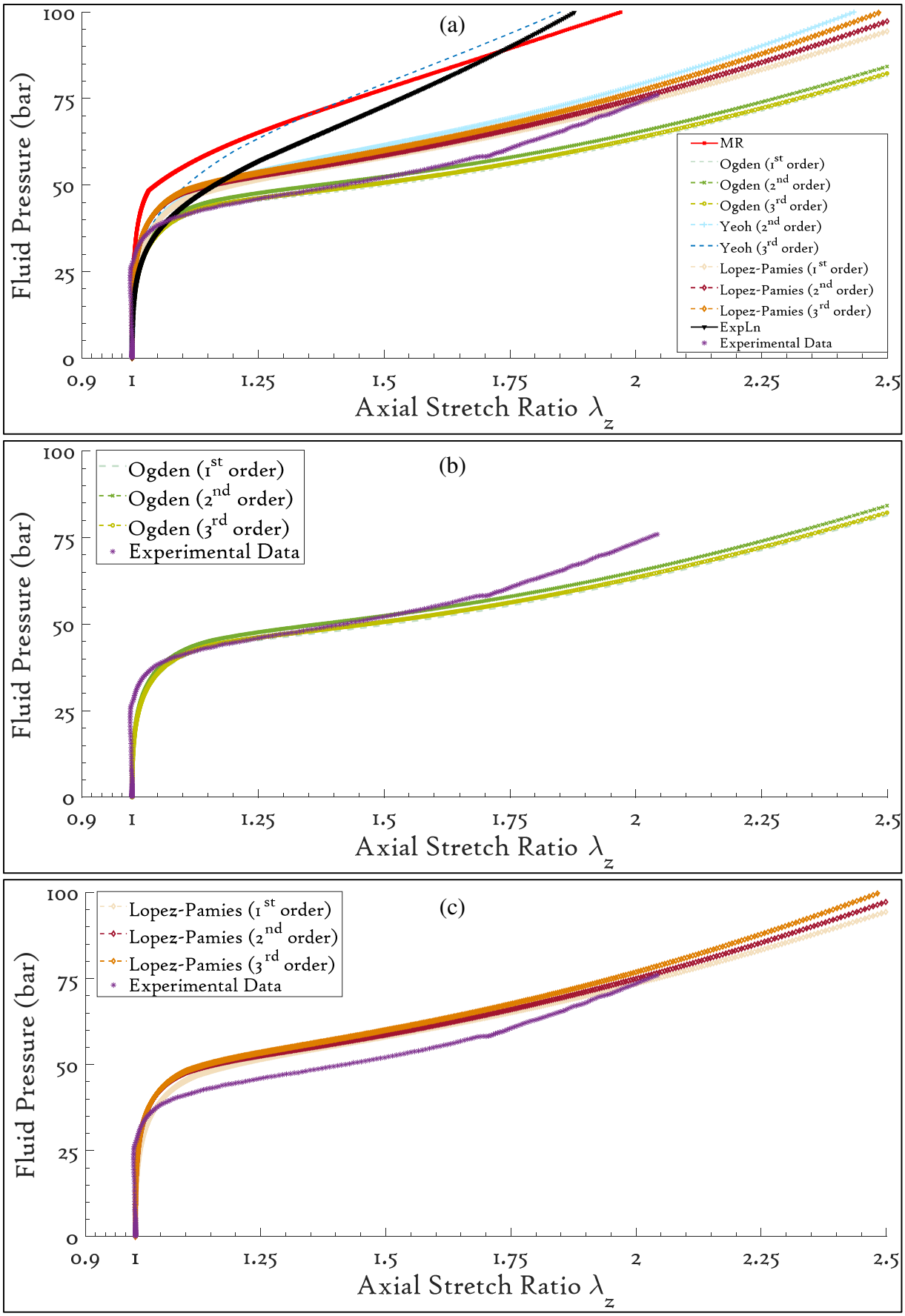

Figure 7: Thick Walled Rubber Cylinder Inflation behaviour compared with the experimental data (a) All 5 hyperelastic models, (b) Ogden models, (c) Lopez-Pamies models

Planar uniaxial tests are not a true representation of the multi-axial inflation loading that the rubber undergoes in RCAIT. However, this study of different hyperelastic models and how they predict inflation behaviour highlights the importance of choosing the appropriate model.

Before moving to the SERR evaluation, the Thick-Walled Cylinder Inflation evolution for each of these models based on the data from *Table 1* should be considered. Following the algorithm described in *Figure 4*, these data can be converted into a *fluid pressure vs specimen axial stretch ratio* evolution. Such a plot is shown in *Figure 7*, compared with the experimental results. The fluid pressure is readily measured during the experiments, whereas the axial stretch ratio is calculated using image processing.

Overall, after a strain of merely *5%* (λ_z*=1.05*), all the curves start diverging. The *ExpLn* and *Yeoh Model (3rd Order)* show considerable strain hardening, especially at *100%* strain. All 3 orders of the *Lopez-Pamies* model follow a parallel trend in the CIS, so do the *Ogden* model curves. However, the behaviour of these models is drastically different in *Figure 7* at large strains. This could be due to the multiaxial loading that the rubber cylinder undergoes in RCAIT. In addition, the presence of the confinement tube adds an extra boundary condition to the rubber inflation which along with the incompressibility of the rubber means that the rubber is forced to stretch more in the axial direction. For the hyperelastic models showing higher strain hardening (*ExpLn* and *Yeoh – 3rd Order*), the fluid pressure increases much more at large strains compared to the other models. These two phenomena together mean that the two models (*ExpLn* and *Yeoh-3rd Order*) predict a larger amount of energy stored in the rubber. This is likely to result in a lower estimate of the SERR (see *Section 2.1*). In the coming section, this effect is studied in detail.

The evolution of the fluid pressure *vs* volume predicted for all 10 cases is shown in *Figure 8*. The plots are also compared with the experimental data shown in *Figure 2*. A clear

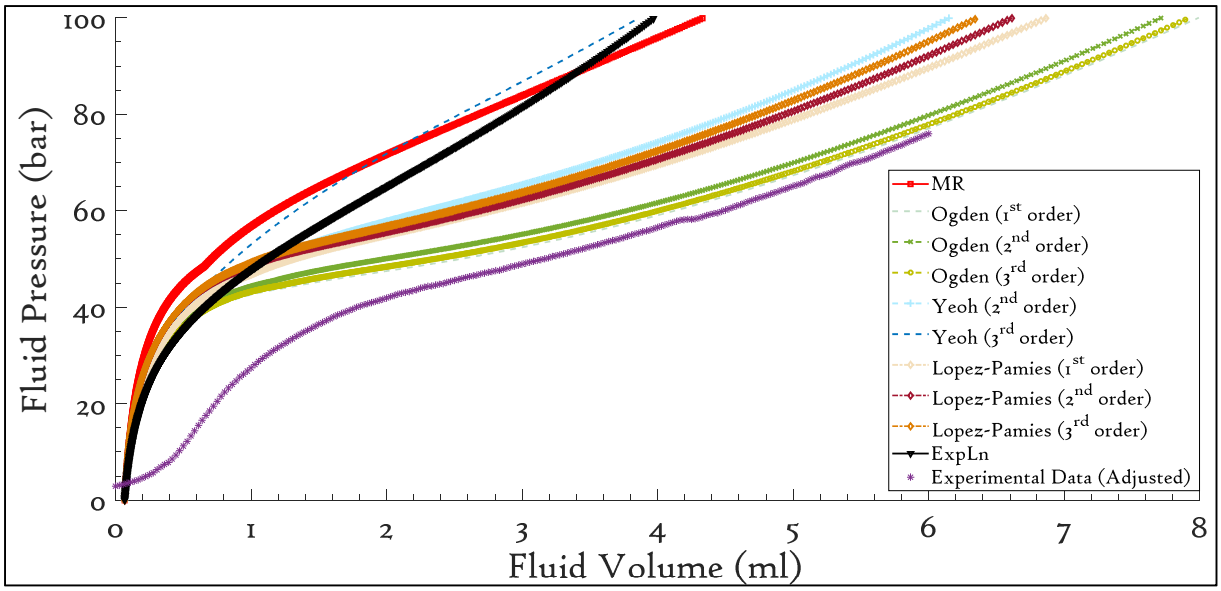

Figure 8: Fluid pressure evolution plotted for all 10 cases and compared with the experimental data. The curve for the experimental data is shifted to the left by 1.5ml to account for initial fluid injection.

disagreement between the prediction and the experimental data is seen. During the experiments, a small initial volume (approx. *1.5ml-2ml*) of liquid must be injected in order to occupy the empty space between the pre-crack length steel cord and rubber envelope. During this stage, the fluid pressure increases only slightly (*5bar-6bar*). The subtraction of this correction (*~1.5ml*) from the injected volume of the experimental data shifts the curve towards the left and the pressure-volume evolution from the experimental data is virtually parallel to that predicted by the *Ogden Models*. Similar behaviour is observed in *Figure 7*.

4.2. Effect of Model on SERR Calculation

Following the general relation of SERR with the test parameters and rubber material parameters described by *(32)*, the SERR can now be calculated for the particular rubber in question. For any given fluid pressure, the deformation state of the rubber cylinder and, as a result, the strain energy stored per unit volume can be calculated using the numerical algorithm described in *Figure 4*. Using *(32)*, the *SERR vs Fluid Pressure* evolution can now be plotted, as seen in *Figure 9*. Similar to *Figure 7*, all the curves follow nearly the same path up to *50bar*. There is a large spread between the curves after that point, as the pressure increases. As predicted earlier, for large strains the models *ExpLn* and *Yeoh (3rd Order)* show

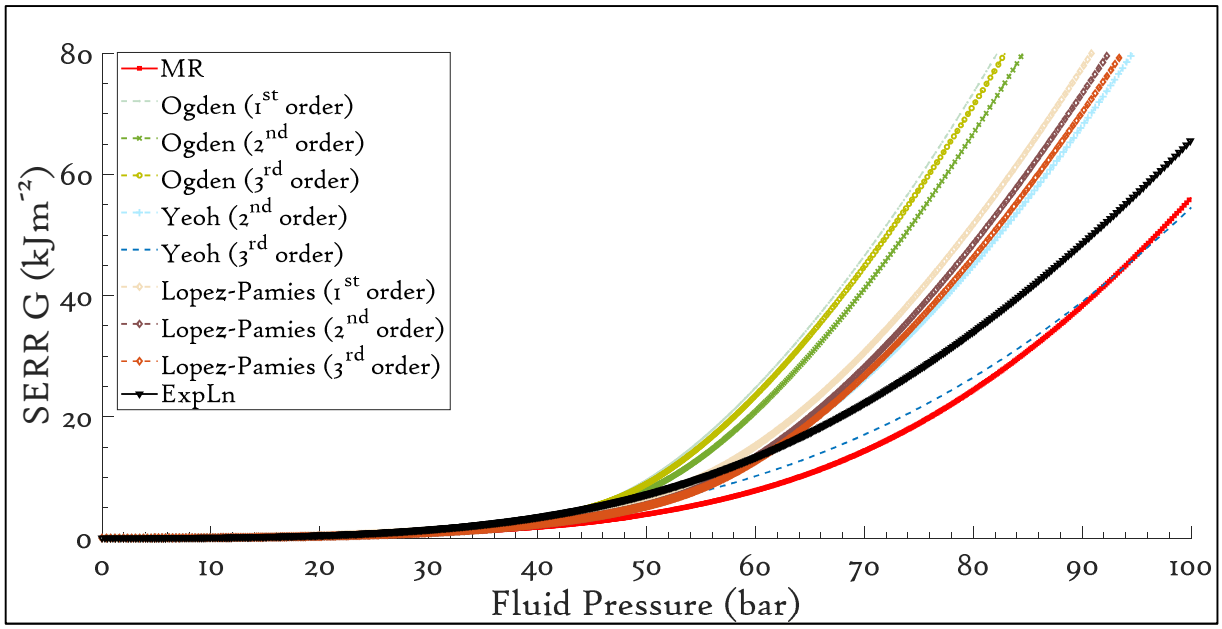

Figure 9: Evaluation of SERR for all 10 cases

a lower estimation of *G*. The curves of the all three orders of *Lopez-Pamies* model follow each other closely even at a pressure up to *90bar*. Similar behaviour is observed for the *Ogden* models as well.

Using *Figure 9* the critical SERR values can be calculated for the test case shown in *Figure 2* at a fluid pressure of *74.9bar*. The results are presented in *Figure 10*. Between the five hyperelastic models the critical SERR value varies within a range of nearly $40kJm^{-2}$. The average value of critical SERR is $38.6\pm13.5kJm^{-2}$. To put this into perspective, a critical SERR value of $27.4kJm^{-2}$ was calculated in *Section 2.1* using a general definition of SERR. This signifies that other dissipation mechanisms might be involved in the crack propagation process. Moreover, the prediction of the $P(\Delta V)$ evolution during the tube inflation experiment may not be reliable due to poor identification procedure and/or choice of a hyperelastic model. Therefore, an alternative material parameter identification procedure is proposed below using the RCAIT data recorded during the inflation phase.

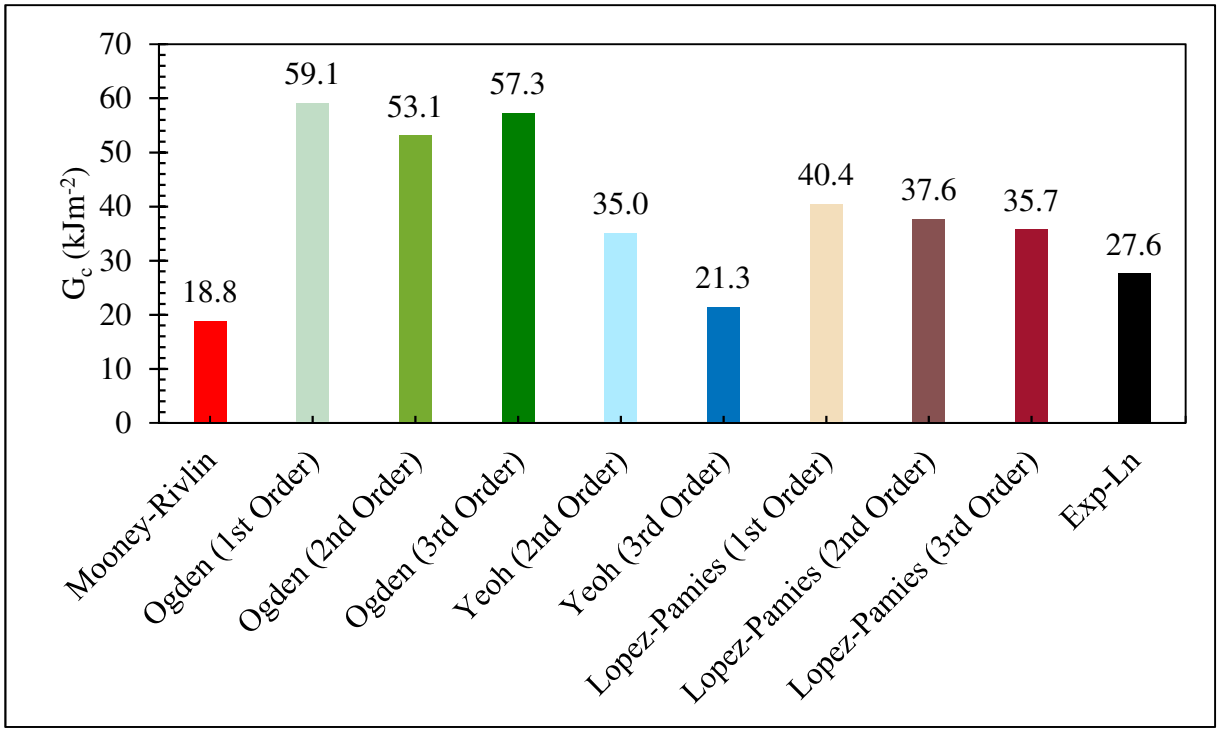

Figure 10: Critical SERR values evaluated for the test case in Figure 2

5. Volumetric Data Fitting

Examining the results presented in the previous section, it is clear that quantitative analysis of how constitutive models affect SERR evaluation is important. It is important to choose such a model wisely and fit the experimental data to obtain precise values of material properties. As explained above, due to a limited availability of the rubber samples for performing complex tests (bi-axial, pure shear etc.), fitting any rubber constitutive model to the data was not easy. However, there is a lot of information concealed in the *pressure vs injected volume* curve, such as *Figure 2*, which can be used to fit the rubber constitutive models. This section focuses on the evaluation of strain energy density parameters for the 10 cases (or five hyperelastic models) using the volumetric data from *Figure 2* and the uniaxial tensile test data.

5.1. Data fitting algorithm

The volumetric data fitting starts with choosing the data from the entire inflation regime in the *pressure vs injected volume* plot (*Figure 2*). Using the values of the injected volume, the deformed inner radius can be calculated from a simple relation

$$r^{int} = \sqrt{\frac{V}{\pi \lambda_z l_p} + r_0^{int^2}} \tag{33}$$

where V is the volume injected and l_p is the pre-crack length of the specimen (*50mm*).

To fit the material parameters of each hyperelastic model using the experimental data (inflation and tensile test data), the following cost function is minimised using the *lsqnonlin* function of *MATLAB*®

$$f_c = \{(P_{int} - P_{exp}) + (\sigma_{model} - \sigma_{tensile})\} \tag{34}$$

Here, P_{int} is the fluid pressure calculated for the specific hyperelastic model using r^{int}, P_{exp} is the fluid pressure recorded during the experiment. σ_{model} is the uniaxial Cauchy stress calculated for the specific hyperelastic model and $\sigma_{tensile}$ is the Cauchy stress recorded during the uniaxial tensile test. Therefore, this volumetric data fitting is aimed at minimising the difference between measured and predicted values of pressure and uniaxial tensile stress while treating the material parameters as the decision variables to be calculated.

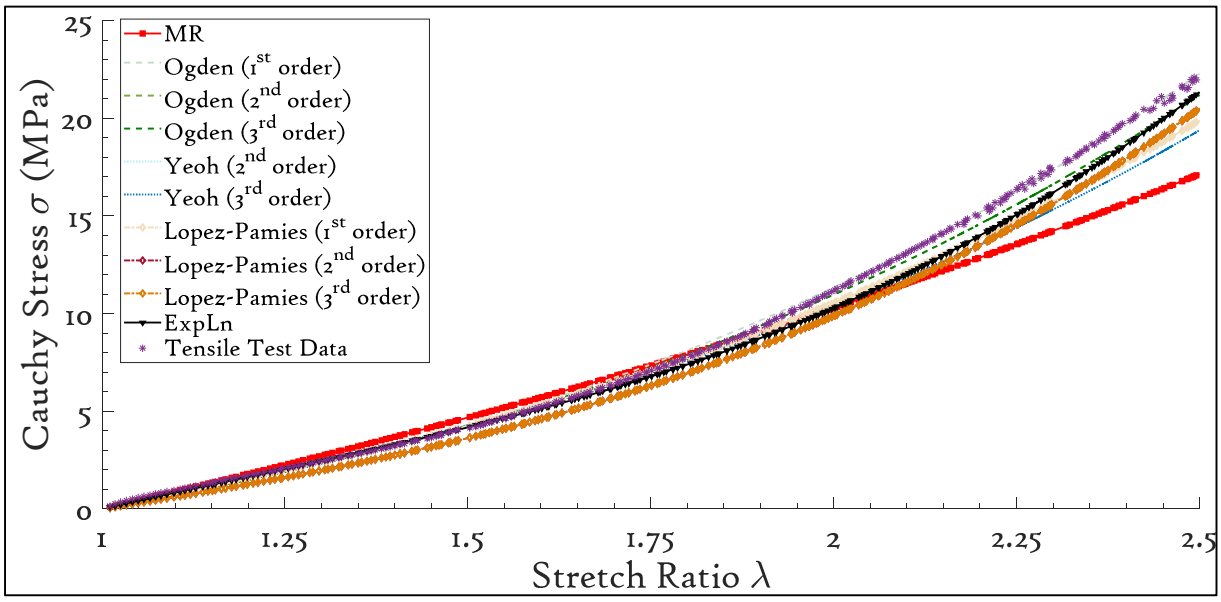

Figure 11: Tensile test data fitting performed using volumetric data

For the test case shown in *Figure 2*, the calculated Cauchy stress values (σ_{model}) from the volumetric data fitting and the values from tensile test data ($\sigma_{tensile}$) are plotted against the axial stretch observed in the tensile tests, in *Figure 11*. Overall, the data fitting seem to be poor compared to the one for purely tensile test data (*Figure 6*). This is expected since the data fitting

Hyperelastic Model	Parameter fit from Volumetric Data and Uniaxial tests	
Mooney-Rivlin	C_1=1.44 MPa	C_2=0.05MPa
Ogden Model (1st Order)	α=2.88	μ=1.62MPa
Ogden Model (2nd Order)	α_1=2.79	μ_1=1.67MPa
	α_2=14.04	μ_2=0.03Pa
Ogden Model (3rd Order)	α_1=2.79	μ_1=1.67MPa
	α_2=14.04	μ_2=0.03Pa
	α_3=2.8	μ_3=8450Pa
Yeoh Model (2nd Order)	C_1=1.31MPa	C_2=0.044MPa
Yeoh Model (3rd Order)	C_1=1.31MPa	C_2=0.044MPa
	C_3=0MPa	
Lopez-Pamies Model (1st Order)	α=1.35	μ=2.52MPa
Lopez-Pamies Model (2nd Order)	α_1=1.62	μ_1=1.06MPa
	α_2=1.62	μ_2=1MPa
Lopez-Pamies Model (3rd Order)	α_1=1.62	μ_1=1.06MPa
	α_2=1.62	μ_2=1MPa
	α_2=1.74	μ_2=72.94Pa
ExpLn	A=1.08MPa a=-0.82	b=-0.97

Table 2: Volumetric data fit to 10 Cauchy stress equations (5 hyperelastic models)

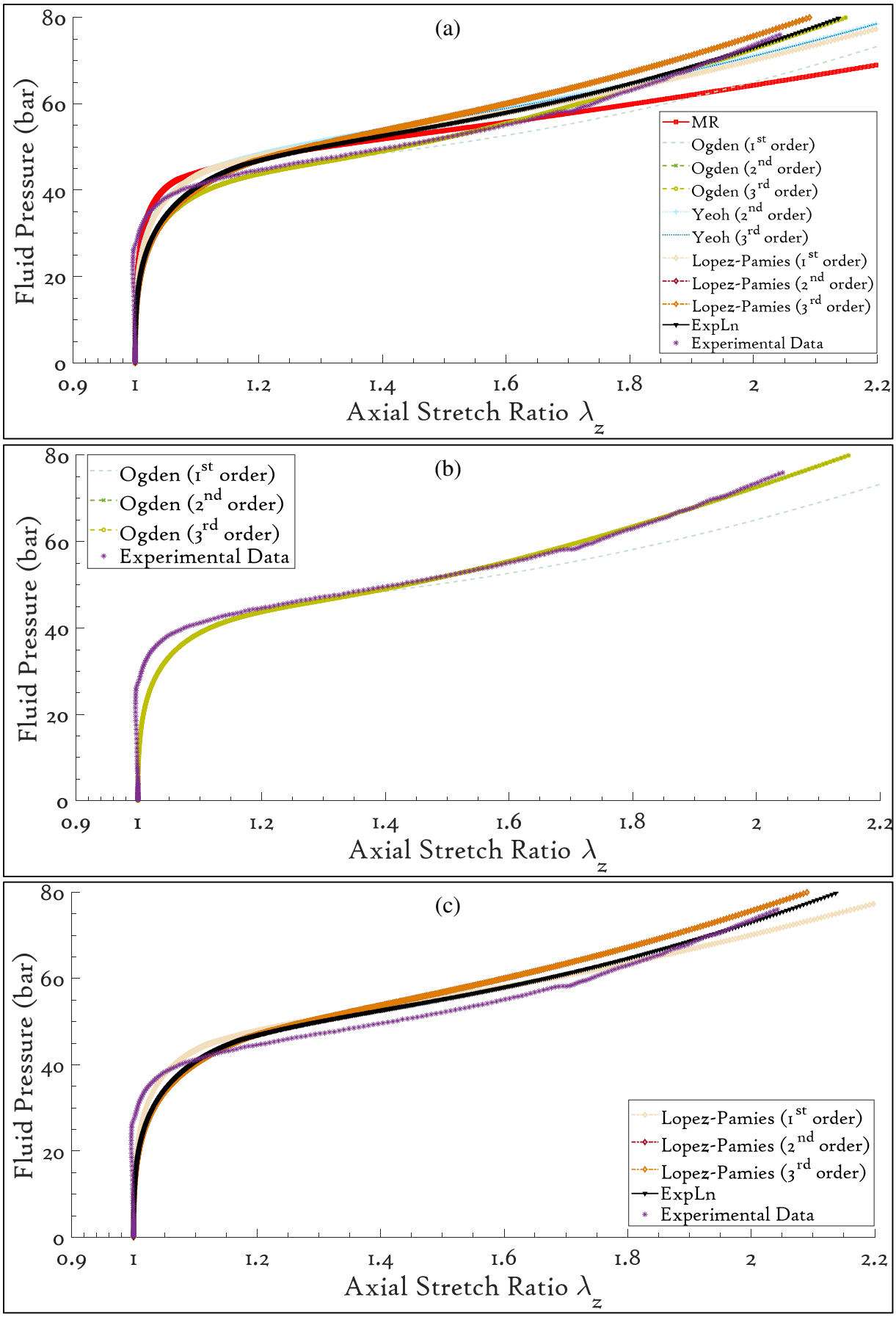

Figure 12: Thick Walled Rubber Cylinder Inflation behaviour from volumetric data fitting. Experimental data is compared with (a) All 5 hyperelastic models, (b) Ogden models, (c) Lopez-Pamies and ExpLn models

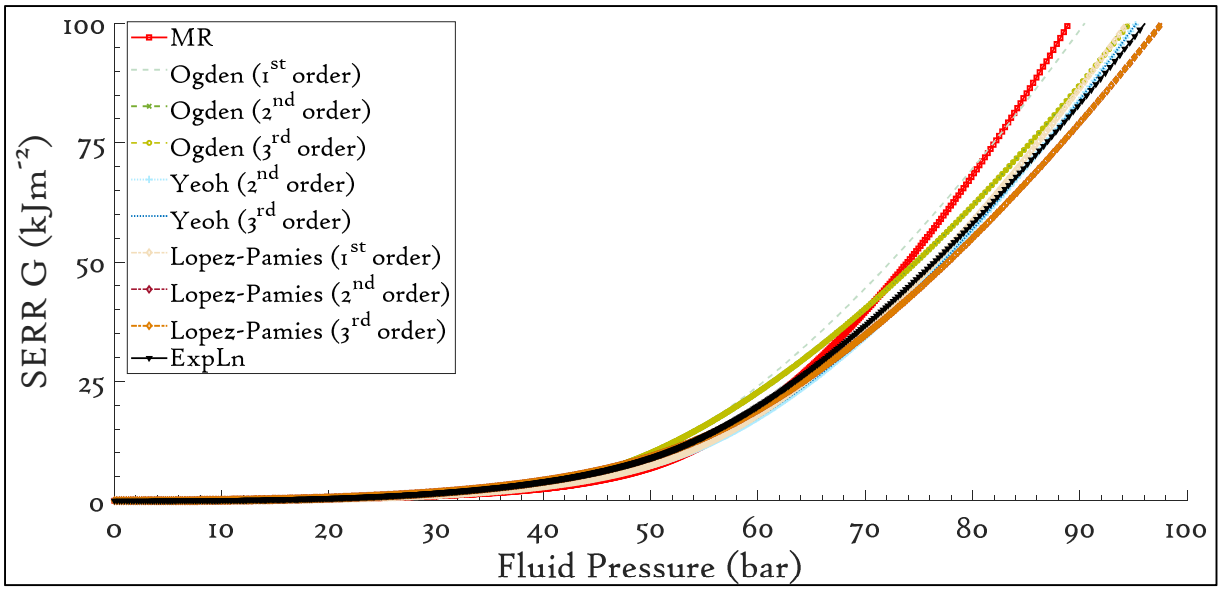

Figure 13: SERR values calculated for 10 cases using volumetric data fitting

also takes into account the volumetric data. The Ogden models, Lopez-Pamies models of the 2nd and 3rd order and the ExpLn model seem to fit the data slightly better than the other models. The strain energy density parameters calculated using this volumetric fitting technique are tabulated in *Table 2*. The material parameter values calculated using volumetric data fitting are different than those in *Table 1*. It is of interest to see how this fitting predicts the volumetric evolution of the specimen.

Using the material parameters shown in *Table 2* in conjunction with the Thick-Walled Cylinder Inflation Model algorithm shown in *Figure 4*, the evolution of *pressure vs axial stretch ratio* (λ_z) is plotted in *Figure 12*. The spread in the inflation behaviour is much smaller than that seen in *Figure 7* indicating a better fit. In particular, the Ogden models of 2nd and 3rd order seem to fit the volumetric data fairly well. The Mooney-Rivlin model fits poorly, especially in the large strain regime.

The SERR values calculated using these material parameters are plotted against fluid pressure in *Figure 13*. Similar to the behaviour seen in *Figure 12*, the SERR curves in *Figure 13* do not show a spread even at *50bar*.

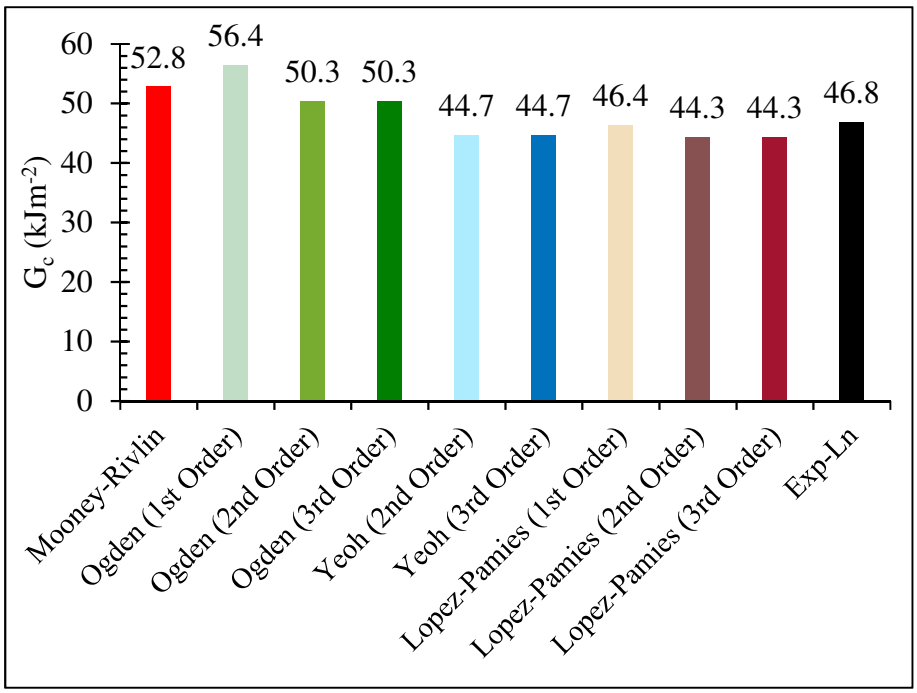

Figure 14: Critical SERR values evaluated using the volumetric data fitting for the test case in Figure 2

Figure 14 shows the critical SERR values evaluated from the curves shown in *Figure 13* and considering the mean crack propagation pressure shown in *Figure 2* i.e. *74.9bar*. The critical SERR values calculated using the volumetric data fitting technique are considerably different from those calculated using tensile test data only (*Figure 10*). As mentioned above, the spread between the values is much smaller, *~12kJm^{-2}*, compared to the *~40kJm^{-2}* spread observed in *Figure 10*. Therefore, the SERR evaluation from volumetric data fitting algorithm is more reliable than that using the tensile test data only. The average critical SERR value is *48.1±3.9kJm^{-2}*. In *Section 2.1*, G_c was calculated to be *27.4kJm^{-2}* using a general definition of SERR. Although the G_c values are of the same order of magnitude, the difference clearly justifies the need to develop the semi-analytical model presented here.

The theoretical work presented in this article can be extended in terms of fracture surface analysis of the test as well. In this context, the fractured steel cord was examined with an X-ray tomography equipment in order to investigate the fractured surfaces. It was found that a *ca. 0.2mm* thick layer of rubber remained on the steel cord at the end of the test (*Figure 15*). The thickness of the brass coating is merely *0.05-0.1µm*. This indicates that the fracture

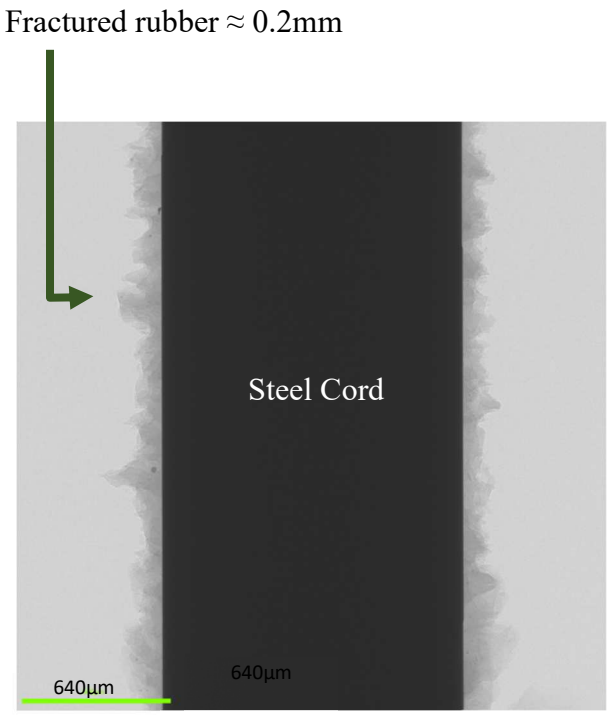

Figure 15: X-ray tomography lateral cross-section of the fractured cord

propagates very close to, but not exactly at the interface. This should be taken into consideration while drawing up the global energy balance. The *0.2mm* should be subtracted from the undeformed rubber thickness to obtain $r^{int}=0.85mm$. This changes the SERR evaluation, however, there is only a minor difference in the SERR values compared to *Figure 14*. The average critical SERR value is $46.5\pm2.2kJm^{-2}$. In reference [11], 90° peel tests on rubber-steel adhesion showed a value of G_c of $\sim30kJm^{-2}$. Although the rubber used in [11] had a lower carbon black content and the fracture was of the stick-slip type, the order of magnitude of the G_c values is the same. An XPS study of the fractured cord surface would reveal more about the failure mode – whether it is adhesive or cohesive.

6. Concluding Remarks

This work focuses on numerical analysis of the Rubber Cord Adhesion Inflation Test (RCAIT). The resolution technique for predicting the inflation of a hyperelastic Thick-Walled Cylinder and applicable to a broad range of hyperelastic models is presented. This model is used to evaluate the theoretical critical SERR (G_c) as a function of the stationary pressure measured during the crack propagation phase of RCAIT. Significant variations are observed

when hyperelastic law parameters are identified from simple tensile test data denoting that the tube inflation behaviour is not properly predicted.

The rubber envelope expansion strongly contributes to the overall energy balance of the crack propagation process, due to the large stretches and multiaxial loading conditions observed during the test. Identifying the rubber behaviour from simple uniaxial tensile test data only is not relevant. Therefore, a volumetric data fitting technique is introduced where pressure-volume data from the inflation tests along with the tensile test data are used to evaluate the rubber behaviour. Using the data from the RCAIT experiment leads to drastic reduction in the dispersion of G_c values with respect to different hyperelastic models. Due to this data reduction technique, G_c evaluation is less sensitive to the rubber mechanical behaviour introduced in the analysis. This approach simply allows better fitting of the $P\Delta V$ evolution needed for the energy balance analysis. Additionally, using such a model is fundamental to evaluate various quantities related to the rubber envelope inflation that will be needed in future work to take into account various dissipative and / or damage phenomena. Now that a reliable G_c evaluation is achieved, supplementary assessment can be achieved by comparing RCAIT test results with peel tests provided that both tests have similar material and loading conditions.

7. Acknowledgement

The authors wish to acknowledge Maxime Daude of MFP Michelin for the supply of RCAIT specimens.

8. References

[1] K. Kane, J. Jumel, F. Lallet, A. Mbiakop-Ngassa, J.-M. Vacherand and M. E. R. Shanahan, "A novel inflation adhesion test for elastomeric matrix / steel cord," *Int. J. Solid. Struct. 160 (2019), 40-50.*

[2] K. Kane, J. Jumel, F. Lallet, A. Mbiakop-Ngassa, J.-M. Vacherand and M. E. R. Shanahan, "Experimental study of the rubber cord adhesion inflation test," *Eng. Fract. Mech. 224 (2020) 106783.*

[3] J. D. Walter, "Cord—Rubber Tire Composites: Theory and Applications," *Rubber Chem Technol, 51(3), 524-576,* 1978.

[4] W. J. van Ooij, "The role of XPS in the study and understanding of Rubber-to-metal bonding," *Surf. Sci. 68 (1977) 1-9.*

[5] A. Lechtenboehmer, H. G. Moneypenny and F. Mersch, "A review of polymer interfaces in tyre technology," *Polymer International, 22(4), 265-301,* 1990.

[6] E. Sarlin, A. Rosling, M. Honkanen, M. Lindgren, M. Juutilainen, M. Poikelispaa, P. Laihonen, M. Vippola and J. Vuorinen, "Effect of environment on bromobutyl rubber-steel adhesion," *Rubber Chem. Technol. 93 (2), 2020, 429-444.*

[7] ASTM D1781-98(2012), Standard Test Method for Climbing Drum Peel for Adhesives, ASTM International, West Conshohocken, PA, 2012, www.astm.org.

[8] ASTM D1871-04(2014), Standard Test Method for Adhesion Between Tire Bead Wire and Rubber, ASTM International, West Conshohocken, PA, 2014, www.astm.org.

[9] ASTM D2229-10(2014), Standard Test Method for Adhesion Between Steel Tire Cords and Rubber, ASTM International, West Conshohocken, PA, 2014, www.astm.org.

[10] ASTM D429-14(2014), Standard test methods for rubber property – adhesion to rigid substrates, ASTM International, West Conshohocken, PA, 2014, www.astm.org.

[11] J. W. Cook, S. Edge and D. E. Packham, "The adhesion of natural rubber to steel and the use of the peel test to study its nature," *Intl. J. Adhes. Adhes. 17(4) (1997) 333-337.*

[12] M. D. Ellul and R. J. Emerson, "A new pull-out test for tire cord adhesion- Part I. Hot Bonding," Rubber Division Meeting, American Chemical Society, October 6-9, Cleveland, Ohio, 1987.

[13] M. D. Ellul and R. J. Emerson, "A new pull-out test for tire cord adhesion- Part II. Cold Bonding," Rubber Division Meeting, American Chemical Society, October 6-9,

Cleveland, Ohio, 1987.

[14] G. S. Fielding-Russell, D. W. Nicholson and D. L. Livingston, “Physical Factors in Cord-to-Rubber Adhesion by a New Tire Cord Adhesion Test,” *Tire Reinforcement and Tire Performance, ed. R. Fleming and D. Livingston (West Conshohocken, PA: ASTM International, 1979), 153-162.*

[15] A. N. Gent and S. Y. Kaang, “Pull-Out and Push-Out Tests for Rubber-to Metal Adhesion,” *Rubber Chem. Technol. 62(4) (1989) 757-766.*

[16] M. Jamshidi, F. Afshar, N. Mohammadi and S. Pourmahdian, “Study on cord/rubber interface at elevated temperatures by H-pull test method,” *Appl. Surf. Sci., 249(1-4) (2005) 208-215.*

[17] F. Teklal, A. Djebbar, S. Allaoui, G. Hivet, Y. Joliff and B. Kacimi, “A review of analytical models to describe pull-out behavior–Fiber/matrix adhesion,” *Compos. Struct. 201 (2018), 791-815.*

[18] H. M. Pekachaki, S. Taghvei-Ganjali, F. Motiee and M. Saber-Tehrani, “Application of calixarene derivatives as tackifier resin in rubber compounds for tire applications,” *Rubber Chem. Technol. 92(3), (2019), 467-480.*

[19] H. Dannenberg, “Measurement of Adhesion by a Blister Method,” *Journal of Applied Polymer Science, 5 (14), 125-134,* 1961.

[20] Y. S. Chang, Y. H. Lai and D. A. Dillard, “The constrained blister—a nearly constant strain energy release rate test for adhesives,” *J. Adhes. 27(4) (1989), 197-211.*

[21] M. J. Napolitano, A. Chudnovsky and A. Moet, “The constrained blister test for the energy of interfacial adhesion,” *J Adhes Sci Technol, 2(1), 311-323,* 1988.

[22] G. Marckmann and E. Verron, “Comparison of hyperelastic models for rubber-like materials,” *Rubber Chem. Technol. 79(5) (2006), 835-858.*

[23] M. Hossain and P. Steinmann, “More hyperelastic models for rubber-like materials: consistent tangent operators and comparative study,” *J. Mech. Behav. Mater. 22 (2012), 1-2.*

[24] H. Darijani and R. Naghdabadi, “Hyperelastic materials behavior modeling using consistent strain energy density functions,” *Acta Mech. 213 (2010), 235-254.*

[25] H. Dal, Y. Badienia, K. Acikgoz and F. A. Denli, “A comparative study on hyperelastic constitutive models on rubber: State of the art after 2006,” in *Proceedings of the 11th European Conference on Constitutive Models for Rubber (ECCMR 2019), June 25-27, 2019*, Nantes, France.

[26] T. Beda, “An approach for hyperelastic model-building and parameters estimation a review of constitutive models,” *Eur. Polym. J. , 50 (2014), 97-108.*

[27] M. Shojaeifard, K. Wang and M. Baghani, “Large deformation of hyperelastic thick-walled vessels under combined extension-torsion-pressure: analytical solution and FEM,” *Mech. Base. Des. Struct. Mach. (2020), 1-18.*

[28] Y. Anani and G. H. Rahimi, “Stress analysis of thick pressure vessel composed of functionally graded incompressible hyperelastic materials,” *Int. J. Mech. Sci. 104 (2015), 1-7.*

[29] D. P. Skala, “Modified Equations of Rubber Elasticity Applied to The Inflation Mechanics of A Thick-Walled Rubber Cylinder,” *Rubber Chem Technol, 43(4), 745-757,* 1970.

[30] L. R. G. Treloar, “Stress-strain data for vulcanised rubber under various types of deformation,” *Trans. Faraday Soc. 40 (1944), 59-70.*

[31] M. Mooney, “A Theory of Large Elastic Deformation,” *J. Appl. Phys. 11 (1940), 582.*

[32] R. W. Ogden, “Large deformation isotropic elasticity – on the correlation of theory and experiment for incompressible rubberlike solids,” *Proc. R. Soc. Lond. A 326 (1997), 565-584.*

[33] O. H. Yeoh, “Some forms of the strain energy function for rubber,” *Rubber Chem. Technol. 66(5) (1993), 754-771.*

[34] O. Lopez-Pamies, “A new I1-based hyperelastic model for rubber elastic materials,” *C. R. Mec. 338 (2010), 3-11.*

[35] H. Khajehsaeid, J. Arghavani and R. Naghdabadi, “A hyperelastic constitutive model for rubber-like materials,” *Eur. J. Mech. A-Solid. 38 (2013), 144-151.*

[36] A. N. Gent, G. S. Fielding-Russell, D. I. Livingston and D. W. Nicholson, “Failure of cord-rubber composites by pull-out or transverse fracture,” *J. Mat. Sci. 16 (1981), 949-956.*

[37] M. H. B. M. Shariff, “Strain Energy Function for Filled and Unfilled Rubberlike Material,” *Rubber Chem. Technol. 73 (1) (2000), 1-18 .*

[38] M. M. Attard and G. W. Hunt, “Hyperelastic constitutive modeling under finite strain,” *Int. J. Solid. Struct. 41 (2004), 5327-5350.*

[39] M. Kaliske and G. Heinrich, “An Extended Tube-Model for Rubber Elasticity: Statistical-Mechanical Theory and Finite Element Implementation,” *Rubber Chem.*

Technol. 72 (4) (1999), 602-632.

[40] P. L. Rosendahl, M. Drass, J. Felger, J. Schneider and W. Becker, “Equivalent strain failure criterion for multiaxially loaded incompressible hyperelastic elastomers,” *Int. J. Solids. Struct. 166 (2019), 32-46.*